

1 Quantifying the contribution of anthropogenic influence to the
2 East Asian winter monsoon in 1960–2012

3
4 Xin Hao^{*1,2}, Shengping He^{4,1}, Huijun Wang^{1,2,3}, Tingting Han^{1,2}

5 ¹ Collaborative Innovation Center on Forecast and Evaluation of Meteorological
6 Disasters/Key Laboratory of Meteorological Disaster, Ministry of Education, Nanjing
7 University for Information Science and Technology, Nanjing 210044, China

8 ² Nansen-Zhu International Research Centre, Institute of Atmospheric Physics, Chinese
9 Academy of Sciences, Beijing 100029, China

10 ³ Climate Change Research Center, Chinese Academy of Sciences, Beijing 100029, China

11 ⁴ Geophysical Institute, University of Bergen and Bjerknes Centre for Climate Research,
12 Bergen 0025, Norway

13
14 Corresponding author: Xin Hao, haoxlike91@163.com

15
16 Abstract

17 The East Asian winter monsoon (EAWM) is greatly influenced by many factors that can be
18 classified as anthropogenic forcing and natural forcing. Here we explore the contribution of
19 anthropogenic influence to the change in the EAWM over the past decades. Under all forcings
20 observed during 1960–2013 (All-Hist run), the atmospheric general circulation model is able to
21 reproduce the climatology and variability of the EAWM-related surface air temperature and 500
22 hPa geopotential height, and shows a statistically significant decreasing EAWM intensity with a
23 trend coefficient of $\sim -0.04 \text{ yr}^{-1}$ which is close to the observed trend. By contrast, the simulation,
24 which is driven by the same forcing as All-Hist run but with the anthropogenic contribution to
25 them removed, shows no decreasing trend in the EAWM intensity. By comparing the simulations
26 under two different forcing scenarios, we further reveal that the responses of the EAWM to the
27 anthropogenic forcing include a rise of 0.6°C in surface air temperature over the East Asia as well
28 as weakening of the East Asia trough, which may result from the poleward expansion and
29 intensification of the East Asian jet forced by the change of temperature gradient in the

30 troposphere. Additionally, compared with the simulation without anthropogenic forcing, the
31 frequency of strong (weak) EAWM occurrence is reduced (increased) by 45% (from 0 to 10/7).
32 These results indicate that the weakening of the EAWM during 1960–2013 may be mainly
33 attributed to the anthropogenic influence.

34 **Key words:** anthropogenic influence, East Asian winter monsoon, contribution

35 1. Introduction

36 The East Asian winter monsoon (EAWM) is one of the most dominant climate
37 systems in East Asia. It greatly affects the disastrous winter weather such as cold
38 waves, snowstorms, air pollutions, and spring duststorms (Li et al., 2016; Li and
39 Wang, 2013; Wang et al., 2009; Zhou et al., 2009; Chang et al., 2006). Prominent
40 circulation components from surface to the upper troposphere associated with
41 temperature condition during the boreal winter are dynamically linked to the EAWM.
42 At surface, the EAWM contains the cold Siberian high dominated over the East Asian
43 continent and the warm Aleutian low located in the high-latitude North Pacific, which
44 accompanies with prevailing northwesterly winds in the low-level troposphere (He
45 and Wang, 2013; Wang and Jiang, 2004; Gong et al., 2001; Guo 1994; Lau and Li,
46 1984). At 500 hPa locates the East Asian trough which determines the outbreak and
47 intensity of the EAWM (He et al., 2013; Cui and Sun, 1999; Sun and Li, 1997). In the
48 upper troposphere, a key component of the EAWM is the East Asian jet with its
49 maximum core being located to the southeast of Japan (Jhun and Lee, 2004; Boyle
50 and Chen, 1987). Concurrent with the change of these atmospheric circulation, the
51 change of winter surface air temperature (SAT) over East Asia is closely related to the
52 variation in the EAWM (Hao and He, 2017; Lee et al., 2013; Wang et al., 2010).

53 The EAWM experienced remarkable transitions, with clear weakening since
54 mid-1980s and re-amplification after mid-2000s (e.g., Yun et al., 2018; Wang and
55 Chen 2014). The decadal oscillations in sea surface temperature (SST) are generally
56 considered as the major source of the decadal variability of the EAWM, such as
57 Pacific decadal oscillation and Atlantic multidecadal oscillation (Hao et al., 2017;
58 Ding et al., 2014; Li and Bates, 2007). Jun and Lee (2004) suggested that the Arctic

59 Oscillation may also contribute to the decadal variability in the EAWM. Additionally,
60 above primary components of the EAWM system are subject to obvious changes
61 under the influence of global warming (e.g., Li et al., 2018; Li et al., 2015; IPCC,
62 2013; Hori and Ueda, 2006; Kimoto, 2005; Zhang et al., 1997). Under different global
63 warming scenarios, thermodynamic contrast between the East Asian continent and the
64 Pacific Ocean is reduced uniformly characterized with weakening of the East Asian
65 trough (EAT) as well as the East Asian jet, indicating a weakening of the EAWM (e.g.,
66 Xu et al., 2016; Kimoto, 2005). Previous studies based on Coupled models generally
67 agree on the effect of global warming on the EAWM (Gong et al., 2018; Miao et al.,
68 2018; Hong et al., 2017; Xu et al., 2016; Kimoto, 2005; Hu et al., 2000). Using the
69 phase 5 of the Coupled Models Intercomparison Project output, Miao et al. (2018)
70 deduced that both increased greenhouse gas concentrations and natural forcings
71 (volcanic aerosols and solar variability) play key roles in the interdecadal weakening
72 of the EAWM in the mid-1980s. However, previous studies mainly conduct
73 qualitative research on the potential influence of the global warming, it's still unclear
74 to what extent can the anthropogenic activities impact the EAWM. This study aims to
75 quantitatively estimate the contribution of increasing anthropogenic emissions over
76 the past decades to the change of the EAWM, which is essential for the projection of
77 the EAWM in the future.

78

79 2. Data and Method

80 Monthly mean dataset including SAT, 500 hPa geopotential height and 250 hPa
81 zonal wind is obtained from National Center for Environmental Prediction/National
82 Center for Atmospheric Research (NCEP/NCAR) Reanalysis 1 dataset at a horizontal
83 resolution of $2.5^\circ \times 2.5^\circ$ (Kalnay et al., 1996). Hereafter it is referred to as
84 “observations”. To explore the contribution of the anthropogenic emissions to climate
85 change, two different simulations from the C20C+ Detection and Attribution Project
86 (<http://portal.nersc.gov/c20c/data.html>) are compared in the context of two different
87 forcing scenarios. One is the *All-Hist* which was forced with time-vary boundary

88 conditions (e.g., greenhouse gas concentrations, anthropogenic and natural aerosols,
89 ozone, solar luminosity, land cover, SSTs and sea ice) observed during the past few
90 decades. The other is the *Nat-Hist* which was forced with observed SST and sea ice
91 concentrations from which the anthropogenic contribution has been removed (please
92 refer to <http://portal.neresc.gov/c20c/data.html> for more details). Meanwhile, the
93 natural external forcing such as greenhouse gas concentrations and aerosols was set to
94 preindustrial levels. We analyse the simulations by an atmospheric general
95 circulation model HadGEM3-A-N216 (Christidis et al., 2013; approximately $0.56^\circ \times$
96 0.83° horizontally) available from the C20C+ Detection and Attribution, which has
97 been used to conduct the above two sets of experiments from 1960 to 2013. Both
98 All-Hist and Nat-Hist runs include 15 ensemble members. Each realization in the two
99 scenarios differs from the other only in its initial state. The ensemble-mean of the runs
100 number 1, 2, 5, 13, 14 and 15 (which show a better performance in simulating
101 interannual, decadal and linear trend change of the EAWM) under the All-Hist
102 scenarios agrees best with the reanalysis dataset (such as climatology, interannual and
103 decadal change of the EAWM; evaluation of other runs of model shown in
104 supplementary). Therefore, the simulations of these 6-members ensemble are used in
105 this study.

106 In this study, we focus on the winter mean which is the average of December,
107 January and February (e.g., the winter 2008 refers to the boreal winter of 2008/2009).
108 Two intensity indices are used to describe the variability of the EAWM: one is defined
109 as the area-averaged height geopotential at 500 hPa in $35^\circ\text{--}45^\circ\text{N}$, $125^\circ\text{--}145^\circ\text{E}$
110 (EAWMI_HGT; Sun and Li, 1997); the other is defined as the area-averaged SAT in
111 $25^\circ\text{--}45^\circ\text{N}$, $105^\circ\text{--}145^\circ\text{E}$ (EAWMI_SAT; Lee et al., 2013). Both area-averaged values
112 are multiplied by -1 so that positive values correspond to strong EAWM; 9-year
113 running mean of the index represents the interdecadal variability of the EAWM.

114

115 3. Results and Discussions

116 3.1 Assessment of the atmospheric circulation pattern simulated by model in All-Hist

117 runs

118 The EAWM is characterized by northerly winds over East Asia, the Siberian high,
119 the Aleutian low, the deep East Asian trough, the upper tropospheric East Asian jet
120 stream, as well as the cold and dry conditions over East Asia (e.g., Hao et al., 2016;
121 Lee et al., 2013; He and Wang, 2013; Wang and Jiang, 2004; Sun and Li, 1997). In
122 this study, the performance of the HadGEM3-A-N216 model in simulating the above
123 characteristics of the EAWM is firstly evaluated by comparing the corresponding
124 results in the All-Hist runs with reanalysis dataset in the period of 1960–2012.

125 Figures 1a-d show the climatology of the SAT and 500 hPa geopotential height
126 in winter from the observations and simulations in the All-Hist run. The winter SAT
127 climatology over East Asia in simulations (Fig. 1a) is generally consistent with the
128 observed counterpart (Fig. 1b). The model has successfully reproduced the dominant
129 features of East Asian winter SAT such as the northwest-to-southeast temperature
130 gradient, the 0°C isotherm of SAT stretching from western China (around 27.5°N)
131 northeastward to north Japan (around 42.5°N), the cold center located over the
132 Tibetan Plateau (Figs. 1a and 1b). Compared with the observations, the simulated SAT
133 shows apparent cold bias over the north of 40°N but less bias over the south of 40°N.
134 In the middle troposphere, the main features (position of axis and intensity) of the
135 EAT are also generally reproduced by the model. The simulated SAT in 25°–45°N,
136 105°–145°E (Lee et al., 2013) and 500 hPa geopotential height in 35°–45°N, 125°–
137 145°E (Sun and Li, 1997) used for the EAWM indices show high spatial correlations
138 with the observations (Fig. 1e), which are exceed 0.99. Additionally, high spatial
139 correlations of the simulated SAT and 500 hPa geopotential height with the
140 observation are accompanied by small root mean square errors (Fig. 1e). It means that
141 the All-Hist runs have well simulated the EAWM climatology.

142 The variability of the EAWM is also compared between the simulations and the
143 observations. It is found that the correlations between the simulated EAWM indices
144 and the observed EAWM indices are 0.3 for EAWMI_SAT and 0.31 for
145 EAWMI_HGT, respectively (Fig. 2), which are statistically significant. Additionally,
146 the interdecadal variability of the EAWM indices are closely correlated between the

147 simulations and the observation with correlation coefficients of 0.7 for EAWMI_SAT
148 and 0.76 for EAWMI_HGT (Fig. 2). The result suggests that the All-Hist runs have
149 well simulated the interannual and interdecadal variability of the EAWM and can be
150 further used to investigate the anthropogenic impact on the EAWM.

151

152 3.2 Contribution of anthropogenic influence to the East Asian winter monsoon

153 To investigate the anthropogenic contribution to the change of the EAWM, we
154 compare the EAWM in the All-Hist runs with those in the Nat-Hist runs. Both of the
155 EAWM indices in the All-Hist runs show statistically significant decreases over the
156 past decades, with trend coefficients of -0.044 (yr^{-1}) and -0.038 (yr^{-1}), respectively,
157 which are similar to the observed trends (-0.023 and -0.02 , respectively; Fig. 2). By
158 contrast, the EAWM indices in Nat-Hist run show an increasing trend, instead (Fig. 2).
159 As shown in Fig. 2, an obviously increasing in EAWMI during 1960-1980 in Nat-Hist
160 runs. The negative phase of Pacific decadal oscillation and Atlantic multidecadal
161 oscillation may be responsible for the enhancing of the EAWM in the Nat-Hist runs
162 during 1960-1980 (Hao et al., 2017; Zhu et al., 2015; Ding et al., 2014). It suggests
163 that the increasing anthropogenic emissions in the past decades may contribute to the
164 weakening of the EAWM.

165 Figure 3 displays the composited differences of the simulated winter SAT and
166 500 hPa geopotential height between the All-Hist runs and in the Nat-Hist runs, which
167 approximately reflect the response of the EAWM to anthropogenic forcing. The
168 composited differences show clearly that winters with anthropogenic forcing see
169 apparent warmer anomalies over most parts of East Asia except for southeast China as
170 well as warmer conditions over the western North Pacific (Fig. 3a). Such a response is
171 similar to the one revealed by previous CMIP5 studies (Hong et al., 2017; Xu et al.
172 2016). Xu et al. (2016) suggested that the large positive anomalies over high-latitude
173 western North Pacific are due to a north ward shift of the significantly intensified
174 Aleutian low induced by the melting sea ice in the Bering Sea and Okhotsk Sea (Gan
175 et al., 2017). Quantitatively, compared with the situation without anthropogenic
176 influence, the wintertime SAT averaged over 20° – 60° N, 100° – 140° E increases by 0.6°C

177 over the last half-century due to anthropogenic influence (Fig. 3a). At middle
178 troposphere, responses of the 500 hPa geopotential height to anthropogenic forcing
179 shows obviously positive anomalies over East Asia with a value of 15.7 m, implying a
180 shallower EAT which results in less powerful cold air to East Asia (Fig. 3b). The
181 model simulations indicate clearly that the anthropogenic influence may induce a
182 weaker EAWM.

183 It should be noted that, in the low-level troposphere, the high-latitude warming
184 induced by the anthropogenic forcing is apparently stronger than the warming at
185 lower-latitudes (Fig. 4a), which is the so-called “polar amplification” (Meehl et al.,
186 2007; Collins et al., 2013). Meanwhile, in the high-level troposphere, obviously
187 warming occurs over the tropical regions and the Arctic, but cooling occurs over
188 mid-latitudes (around 50°N) under the anthropogenic influence (Fig. 4a). As a result,
189 a broadening and intensifying Hadley circulation appears, which is consistent with the
190 observed phenomena revealed by previous studies that a poleward expansion and
191 intensification of the winter Hadley circulation in the past few decades (Hu and Fu,
192 2007; Mitas and Clement, 2005; Hu et al., 2005). Such a change in the Hadley
193 circulation implies a poleward shift of the East Asian jet (Fig. 4b), together with a
194 reinforcement and expansion of Western Pacific subtropical high and a decrease of
195 SLP in northwest China, the sea of Okhotsk, Bering sea and Gulf of Alaska (Fig. 4c).
196 The change of SLP also indicates a weak decrease of the Siberian high and an
197 intensified Aleutian low. Thus, under the anthropogenic influence, significant easterly
198 anomalies occur in the mid- and high-latitude of East Asia and significant southerly
199 anomalies occur in the low-latitude of East Asia (Fig. 4c), leading to a subdued
200 EAWM. We further explore the contribution of anthropogenic influence to the
201 occurrence of strong/weak EAWM. The case with the normalized index larger than
202 1.0 (smaller than -1.0) is defined as a strong (weak) EAWM event. The number of the
203 strong/weak EAWM events is shown in Fig. 5. The two observed EAWM indices
204 display 10 (8) and 9 (9) strong (weak) EAWM events during 1960–2012, respectively.
205 Two simulated EAWM indices in the All-Hist run display 11 (10) and 11 (7) strong
206 (weak) EAWM events, respectively. The number of strong or weak EAWM events

207 forced by the observed time-varying boundary conditions during the past few decades
208 (All-Hist run) is very close to the number in observations. However, during 1960–
209 2012, the simulated two EAWM indices in the Nat-Hist runs display 21 (0) and 19 (0)
210 strong (weak) EAWM events, which is remarkably different from the number in the
211 All-Hist runs as well as the observations. It implies that, in the past decades, the
212 frequency of occurrence of strong EAWM may have reduced by 45% due to the
213 anthropogenic forcing and the anthropogenic forcing is a dominant contributor to the
214 occurrence of weak EAWM.

215 Note that, there is uncertainty of the EAWM simulated by the Nat-Hist runs. A
216 long-term warming occurred in global SST under the influence of global warming
217 over the past decadal (Fig. 6c), causing a weakened EAWM (Hao et al., 2018). We
218 processed the difference of SST forcing between the All-Hist runs and Nat-Hist runs
219 by empirical orthogonal function analysis as EOF1 (Fig. 6a) and associated principal
220 component 1 (Fig. 6b). The first leading mode shows a long-term oceanic warming
221 with explained variance of 91.4%, characterized by negative anomalies in
222 high-latitude oceans of the southern hemisphere, positive anomalies in tropical oceans
223 and mid-latitude oceans of the southern hemisphere and intense positive anomalies in
224 the high-latitude oceans around 60° N. It shows similar intensity and characteristics to
225 the observed warming over global oceans. However, a cooling occurred in the
226 northern Pacific and an obvious warming over Kuroshio region, which didn't capture
227 by the models, may weaken the EAWM (Sun et al., 2016). This difference may induce
228 an underestimation of the EAWM in Nat-Hist runs.

229

230 4 Conclusion

231 The contribution of the anthropogenic influence to the climatology, trends, and
232 the frequency of occurrence of strong/weak EAWM is explored in this study based on
233 numerical simulations. Firstly, we evaluate the performance of the climate model
234 (HadGEM3-A-N216) in simulating the climatology of wintertime circulation over
235 East Asia and variation of EAWM indices during 1960–2012. The winter-mean states

236 of SAT and 500 hPa geopotential height related to the EAWM in the All-Hist runs
237 resemble well those in observation with spatial correlation coefficients of greater than
238 0.99. Also, the interannual and interdecadal variations of the EAWMI_HGT and
239 EAWMI_SAT can be well reproduced by the model under All-Hist scenario. Because
240 of the well performance of the All-His runs in simulating the EAWM indices and
241 winter-mean atmospheric circulation over the East Asia, the exploration about
242 changes of the EAWM induced by anthropogenic influence is considered reliable.

243 Under All-Hist scenario, the EAWM indices have significantly decline trends
244 over the past decades, which are consistent with those in observations, indicating that
245 the weakening of the EAWM could be simulated by the climate model with all forcing.
246 However, the EAWM indices do not have such trends in the Nat-Hist runs. Compared
247 the area-averaged SAT and 500 hPa geopotential height related to the EAWM for the
248 period of 1960–2012 between two families of experiments, it is found that
249 anthropogenic emissions induce obviously positive SAT anomalies in the most region
250 of East Asia and a weakened EAT, as shown in previous results (Hu et al., 2000; Hori
251 and Ueda, 2006; Xu et al. 2016; Hong et al., 2017; Hong et al., 2017). Additionally,
252 11 (11) strong EAWM events and 10 (7) weak EAWM events are forced by All-Hist
253 scenario during 1960–2012, which are close to the frequency of occurrence of strong
254 and weak EAWM in observations, while 21 (19) strong EAWM events and 0 (0) weak
255 EAWM event are forced by Nat-Hist scenario. Overall, under anthropogenic influence,
256 during 1960–2012, the EAWM continued to be weakened, and the frequency of
257 occurrence of strong (weak) EAWM had decreased (increased) by 45% (from 0 to
258 10/7). The poleward expansion and intensification of East Asian jet induced by
259 anthropogenic influence may be the reason for the weakening of the EAWM. A
260 decrease trend is found both in observation and in the All-Hist runs, therefore more
261 attention should be given to the EAWM variability under anthropogenic influence.

262

263 **Author contributions.** Xin Hao conceived the idea for the study and wrote the paper.
264 All authors contributed to the development of the method and to the data analysis.

265 **Acknowledgements**

266 This work was supported by the National Science Foundation of China (Grant
267 41421004, 41875118, 41605059 and 41505073). All datasets can be accessed publicly.
268 The NCEP analysis dataset can be downloaded from
269 <https://www.esrl.noaa.gov/psd/data>, and the simulations can be downloaded from
270 <http://portal.nersc.gov/c20c/data.html>.

271

272

273 References:

274 Boyle, J. S., and Chen, T. J.: Synoptic aspects of the wintertime East Asian monsoon,
275 in: *Monsoon Meteorology*, edited by: Chang, C. P. and Krishnamurti, T. N.,
276 Oxford University Press, 125–160, 1987.

277 Cui, X. P., and Sun, Z. B.: East Asian winter monsoon index and its variation analysis.
278 *J. Nanjing Inst. Meteo.*, 22, 321–325, 1999. (in Chinese)

279 Chang, C. P., Wang, Z., and Hendong, H.: The Asian winter monsoon, in: *The Asian*
280 *Monsoon*, edited by Wang, B., Springer Press, 89–127, 2006.

281 Christidis, N., Stott, P. A., Scaife, A. A., Arribas, A., Jones, G. S., Copsey, D., Knight,
282 J. R., and Tennant, W.J.: A new HadGEM3-A-based system for attribution of
283 weather- and climate-related extreme events, *J. Climate*, 26, 2756–2783.
284 doi: 10.1175/JCLI-D-12-00169.1, 2013.

285 Collins, M., Knutti, R., Arblaster, J., Dufresne, J. L., Fichefet, T., Friedlingstein, P.,
286 Gao, X., Gutowski, W. J., Johns, T., Krinner, G., Shongwe, M., Tebaldi, C.,
287 Weaver, A. J., and Wehner, M.: Long-term climate change: projections,
288 commitments and irreversibility, In: *Climate Change 2013: The Physical Science*
289 *Basis*, Contribution of Working Group I to the Fifth Assessment Report of the
290 Intergovernmental Panel on Climate Change, edited by Stocker, T. F., Qin, D.,
291 Plattner, G. K., Tignor, M., Allen, S. K., Boschung, J., Nauels, A., Xia, Y., Bex,
292 V., and Midgley, P. M., Cambridge University Press, Cambridge, UK and New
293 York, NY, 2013.

294 Ding, Y. H., Liu, Y., Liang S., Ma, X., Zhang, Y., Si, D., Liang, P., Song, Y., and
295 Zhang, J.: Interdecadal variability of the East Asian winter monsoon and its

296 possible links to global climate change. *J. Meteor. Res.*, 28, 693–713, 2014.

297 Gan, B. L., Wu, L. X., Jia, F., Li, S. J., Cai, W. J., Nakamura, H., Alexander, M. A.,
298 and Milley, A. J.: On the response of the Aleutian Low to Greenhouse Warming,
299 *J. Climate*, 30, 3907–3925. 2017.

300 Gong, D. Y., Wang, S. W., and Zhu, J. H.: East Asian winter monsoon and Arctic
301 Oscillation. *Geophys. Res. Lett.*, 28, 2073–2076, 2001.

302 Gong, H. N., Wang L., Zhou W., Chen W., Wu R. G., Liu L., Nath D., and Leung M. Y.
303 T.: Revisiting the northern mode of East Asian winter monsoon variation and its
304 response to global warming. *J. Climate*, 31, 9001–9014, 2018.

305 Guo, Q. Y.: Relationship between the variations of East Asian winter monsoon and
306 temperature anomalies in China. *Q. J. Appl. Meteorol.*, 5, 218–225, 1994. (in
307 Chinese)

308 Hao, X., Li, F., Sun, J. Q., Wang, H. J., and He, S. P.: Assessment of the response of
309 the East Asian winter monsoon to ENSO-like SSTAs in three U.S. CLIVAR
310 Project models. *Inter. J. Climatol.*, 36, 847–866, 2016.

311 Hao, X., and He, S. P.: Combined effect of ENSO-like and Atlantic Multidecadal
312 Oscillation on the interannual variability of the East Asian winter monsoon. *J.*
313 *Climate*, 30, 2697–2716, 2017.

314 He, S. P., Wang, H. J., and Liu, J.: Changes in the relationship between ENSO and
315 Asia-Pacific midlatitude winter atmospheric circulation, *J. Climate*, 26, 3377–
316 3393, 2013.

317 Hao, X., He, S. P., Han, T. T., and Wang, H. J.: Impact of global oceanic warming on
318 winter Eurasian climate. *Adv. Atmos. Sci.*, 35, 1254–1264, 2018.

319 He, S. P., and Wang, H. J.: Oscillating relationship between the East Asian winter
320 monsoon and ENSO, *J. Climate*, 26, 9819–9838, 2013.

321 Hong, J. Y., Ahn, J. B., and Jhun, J. G.: Winter climate changes over East Asian region
322 under RCP scenarios using East Asian winter monsoon indices, *Clim. Dyn.*, 48,
323 577–595, doi:10.1007/s00382-016-3096-5, 2017.

324 Hu, Z. Z., Bengtsson, L., and Arpe, K.: Impact of global warming on the Asian winter
325 monsoon in a coupled GCM. *J. Geophys. Res.*, 105, 4607–4624.

326 doi:10.1029/1999JD901031, 2000.

327 Hu, Y., and Fu, Q.: Observed poleward expansion of the Hadley circulation since
328 1979. *Atmos. Chem. Phys.*, 7, 5229–5236, 2007.

329 Hu, Y., Tung, K. K., and Liu, J.: A closer comparison of early and late winter
330 atmospheric trends in the Northern-Hemisphere, *J. Climate*, 18, 2924–2936,
331 2005.

332 Hori, ME., and Ueda, H.: Impact of global warming on the East Asian winter
333 monsoon as revealed by nine coupled atmosphere ocean GCMs. *Geophys. Res.
334 Lett.*, 33, L03713. doi:10.1029/2005GL024961, 2006.

335 Intergovernmental Panel on Climate Change (IPCC): *Climate Change 2013: The
336 Physical Science Basis, Contribution of Working Group I to the Fifth Assessment
337 Report of the Intergovernmental Panel on Climate Change*, Stocker, T. F., Qin, D.,
338 Plattner, G. K., Tignor, M., Allen, S. K., Boschung, J., Nauels, A., Xia, Y., Bex,
339 V., and Midgley, P. M., Cambridge University Press, Cambridge, UK, 2013.

340 Jhun, J. G., and Lee, E. J.: A new East Asian winter monsoon index and associated
341 characteristics of the winter monsoon. *J. Climate*, 17, 711–726, 2004.

342 Jiang, Y., Yang, X. Q., Liu, X., Yang, D., Sun, X., Wang, M., Ding, A., Wang, T., and
343 Fu, C.: Anthropogenic aerosol effects on East Asian winter monsoon: The role of
344 black carbon-induced Tibetan Plateau warming, *J. Geophys. Res. Atmos.* 122,
345 doi:10.1002/2016JD026237, 2017.

346 Kalnay, E., Kanamitsu, M., Kistler, R., Collins, W., Deaven, D., Gandin, L., Iredell,
347 M., Saha, S., White, G., Woollen, J., Zhu, Y., Chelliah, M., Ebisuzaki, W.,
348 Higgins, W., Janowiak, J., Mo, K. C., Ropelewski, C., Wang, J., Leetmaa, A.,
349 Reynolds, R., Jenne, R., and Joseph, D.: The NCEP/NCAR 40-year reanalysis
350 project, *Bull. Amer. Meteorol. Soc.*, 77, 437–470, 1996.

351 Kimoto, M.: Simulated change of the east Asian circulation under global warming
352 scenario, *Geophys. Res. Lett.*, 32, L16701, doi:10.1029/2005GL023383, 2005.

353 Lau, K. M., and Li, M. T.: The monsoon of East Asia and its global associations-A
354 survey, *Bull. Amer. Meteorol. Soc.*, 65, 114–125, 1984.

355 Lee, S. S., Kim, S. H., Jhun, J. G., Ha, K. J., and Seo, Y. W.: Robust warming over

356 East Asia during the boreal winter monsoon and its possible causes, *Environ. Res.*
357 *Lett.*, 8:034001(6pp), 2013.

358 Li, F., Wang, H. J., and Gao, Y. Q.: Change in sea ice cover is responsible for
359 non-uniform variation in winter temperature over East Asia, *Atmos. Ocean. Sci.*
360 *Lett.*, 8, 376–382, 2015.

361 Li, F., and Wang, H. J.: Relationship between Bering sea ice cover and East Asian
362 winter monsoon year-to-year variations, *Adv. Atmos. Sci.*, 30, 48–56, 2013.

363 Li, Q., Zhang, R. H., and Wang, Y.: Interannual variation of the wintertime fog-haze
364 days across central and eastern China and its relation with East Asian winter
365 monsoon, *Int. J. Climatol.*, 36, 346–354, 2016.

366 Li, S., He, S. P., Li, F., and Wang, H. J.: Simulated and projected relationship between
367 the East Asian winter monsoon and winter Arctic Oscillation in CMIP5 models,
368 *Atmos. Ocean. Sci. Lett.*, 11, 417–424, 2018.

369 Li, S. L., and Bates, G. T.: Influence of the Atlantic multidecadal oscillation on the
370 winter climate of East China. *Adv. Atmos. Sci.*, 24, 126–135, 2007.

371 Meehl, G. A., Stocker, T. F., Collins, W. D., Friedlingstein, P., Gaye, A. T., Gregory, J.
372 M., Kitoh, A., Knutti, R., Murphy, J. M., Noda, A., Raper, S. C. B., Watterson, I.
373 G., Weaver, A. J., and Zhao, Z. C.: Global climate projections, In: *Climate*
374 *Change 2007: The Physical Science Basis, Contribution of Working Group I to*
375 *the Fourth Assessment Report of the Intergovernmental Panel on Climate*
376 *Change*, edited by Solomon, S., Qin, D., Manning, M., Chen, Z., Marquis, M.,
377 Averyt, K. B., Tignor, M., and Miller, H. L., Cambridge University Press,
378 Cambridge, UK and New York, NY, 2007.

379 Miao, J. P., Wang, T., Wang, H. J., Zhu, Y. L., Sun J. Q.: Interdecadal weakening of
380 the East Asian winter monsoon in the mid-1980s: The roles of external forcings,
381 *J. Climate*, 31, 8985–9000, 2018.

382 Mitas, C. M., and Clement, A.: Has the Hadley cell been strengthening in recent
383 decades? *Geophys. Res. Lett.*, 32, L03809, doi:10.1029/2004GL021765, 2005.

384 Sun, B. M., and Li, C. Y.: Relationship between the disturbances of East Asian trough
385 and tropical convective activities in boreal winter. *Chinese Sci. Bull.*, 42, 500–

386 504, 1997. (in Chinese)

387 Wang, B., Wu, Z. W., Chang, C. P., Liu, J., LI, J. P., and Zhou, T. J.: Another Look at
388 interannual-to-interdecadal variations of the East Asian winter monsoon: the
389 northern and southern temperature modes, *J. Climate*, 23, 1495–1512, 2010.

390 Wang, H. J., and Jiang, D. B.: A new East Asian winter monsoon intensity index and
391 atmospheric circulation comparison between strong and weak composite.
392 *Quaternary Sci.*, 24, 19–27, 2004. (in Chinese)

393 Wang, L., Huang, R. H., Gu, L., Chen, W., and Kang, L. H.: Interdecadal Variations of
394 the East Asian winter monsoon and their association with quasi-stationary
395 planetary wave activity, *J. Climate*, 22, 4860–4872, 2009.

396 Wang, L., and Chen, W.: The East Asian winter monsoon: Re-amplification in the
397 mid-2000s, *Chinese Sci. Bull.*, 59, 430–436, 2014.

398 Xu, M. M., Xu, H. M., and Ma, J.: Responses of the East Asian winter monsoon to
399 global warming in CMIP5 models, *Int. J. Climatol.*, 36, 2139–2155,
400 doi:10.1002/joc.4480, 2016.

401 Yun, J. H., Ha, K. J., and Jo, Y. H.: Interdecadal changes in winter surface air
402 temperature over East Asia and their possible causes, *Clim. Dyn.*, 51, 1375–1390,
403 2018.

404 Zhang, Y., Sperber, K. R., Boyle, J. S., Dix, M., Ferranti, L., Kitoh, A., Lau, K. M.,
405 Miyakoda, K., Randall, D., Takacs, L., and Wetherald, R.: East Asian winter
406 monsoon: Results from eight AMIP models, *Clim. Dyn.*, 13, 797–820, 1997.

407 Zhou, W., Chan, C. L. J., Chen, W., Ling, J., Pinto, J. G., and Shao, Y. P.:
408 Synoptic-scale controls of persistent low temperature and icy weather over
409 southern China in January 2008, *Mon. Weather Rev.*, 137, 3978–3991, 2009.

410 Zhu, Y., Wang, H. J., Ma, J. H., Wang, T., Sun, J.: Contribution of the phase transition
411 of Pacific Decadal Oscillation to the late 1990s’ shift in east china summer
412 rainfall. *J. Geophys. Res.* 120, 8817–8827, 2015.

413

414 Figure caption:

415

416 Figure 1 Climatology of winter-mean (DJF) (a) surface air temperature (shading, °C)
417 (c) 500 hPa geopotential height (shading, m) during 1960–2012, based on NCEP
418 reanalysis data. (b), (d) As in (a), (b), but for the model’s All-Hist runs. (e)
419 Taylor diagram of winter-mean climatology for surface air temperature (TAS;
420 25°–45°N, 105°–145°E) and 500 hPa geopotential height (H500; 25°–45°N,
421 105°–145°E). The rectangle marks the areas used to calculate the climatology in
422 taylor diagram.

423

424 Figure 2 (a) The time series of the normalized EAWMI_SAT (curve) and their linear
425 trend (line) during 1960–2012, based on NCEP reanalysis dataset (top), outputs
426 of model in All-Hist run (middle), and outputs of models in Nat-Hist run
427 (bottom). (b) As in (a), but for the EAWMI_HGT. “tr” is an abbreviation for
428 “linear trend coefficient”. “*” means the tr is significant at 95% confidence level
429 based on the Mann-Kendall test, and “’ ” means the tr is significant at 90%
430 confidence level. “cor” is an abbreviation for “correlation coefficient between
431 simulated EAWM index under All-Hist scenario and observed EAWM index”,
432 “cor_dec” is an abbreviation for “correlation coefficient in decadal time-scale”.
433 Note that the time series of the EAWM indices base on outputs of model in the
434 Nat-Hist runs are standardized by the climatology simulated by the All-Hist runs.

435

436 Figure 3 Composite differences of winter-mean (a) surface air temperature
437 (shading, °C) and (b) 500 hPa geopotential height (shading, m) between the
438 All-Hist runs and Nat-Hist runs, during 1960–2012. The plus signs denotes
439 where the composite differences are significant at the 95% confidence level
440 based on two-sided Student *t* test.

441

442 Figure 4 Composite differences of winter-mean (a) air temperature (shading, °C) over
443 90°E–150°E, (b) 250 hPa zonal wind (shading, m/s) and (c) sea level pressure
444 (shading, hPa) and 850 hPa wind (vector, m/s) between the All-Hist runs and
445 Nat-Hist runs, during 1960–2012. Red contours denote the climatology of

446 All-Hist runs. The plus signs denotes where the composite differences are
 447 significant at the 95% confidence level based on two-sided Student t test.

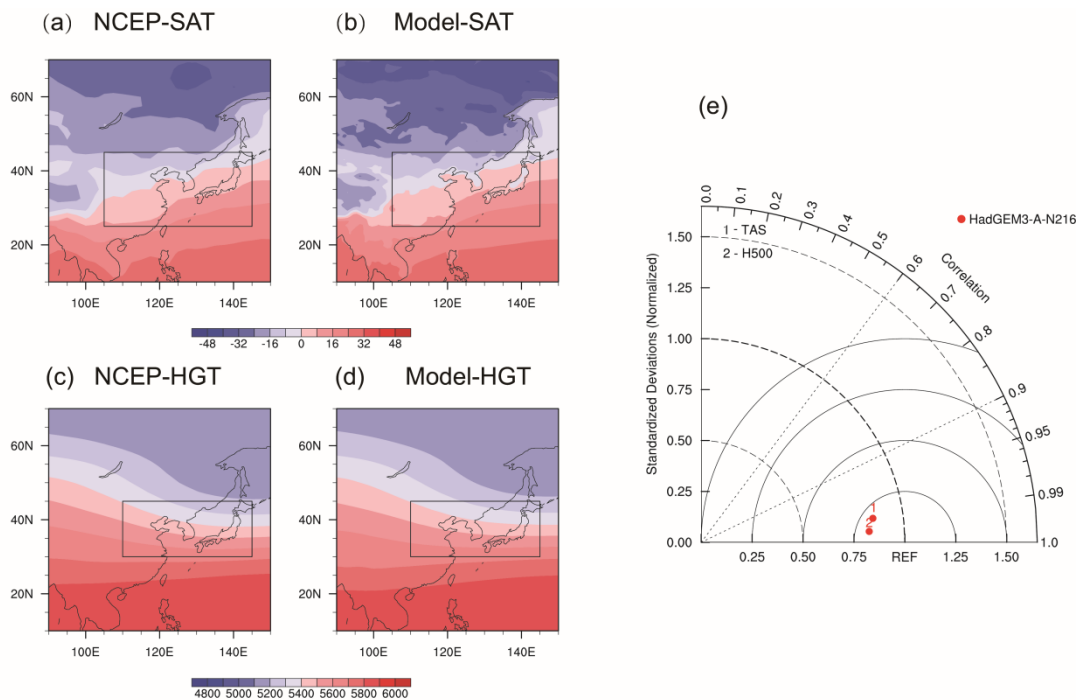
448

449 Figure 5 (a) The number of strong EAWM events during 1960–2012, based on NCEP
 450 reanalysis dataset (left), outputs of model in the All-Hist runs (middle), and
 451 outputs of model in the Nat-Hist runs (right). (b) As in (a), but for weak EAWM
 452 events.

453 Figure 6 The first leading mode (EOF1; a) and associated principal component (PC1;
 454 b) of the difference of the winter-mean sea surface temperature forcing between
 455 the All-Hist runs and Nat-Hist runs by empirical orthogonal function analysis
 456 based on the period of 1960-2013. The second leading mode (REOF2; c) and
 457 associated principal component (RCP2; d) of the winter-mean sea surface
 458 temperature from the HadISST data by rotated empirical orthogonal function
 459 analysis based on period of 1960-2013.

460

461 Figures

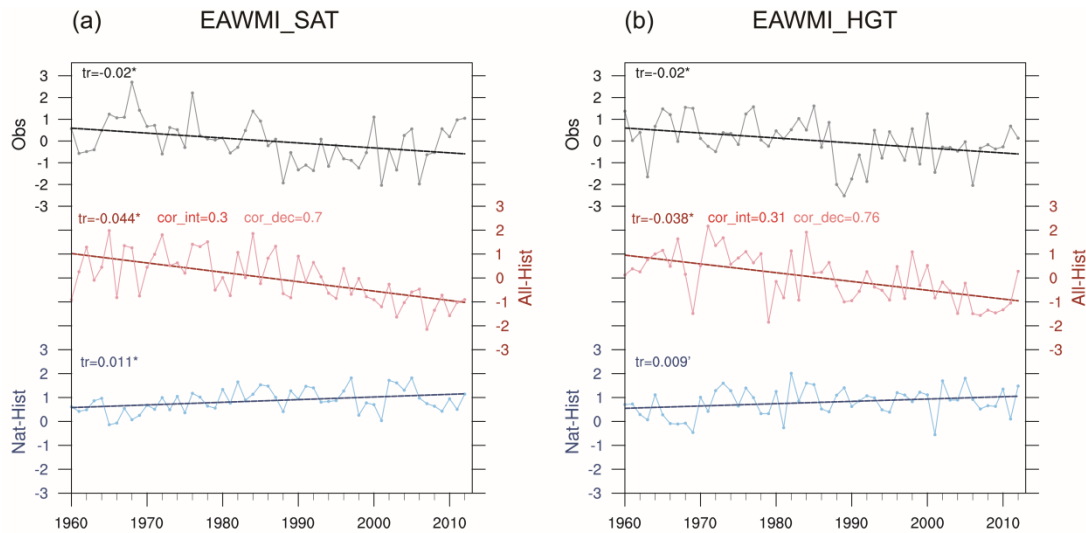


462

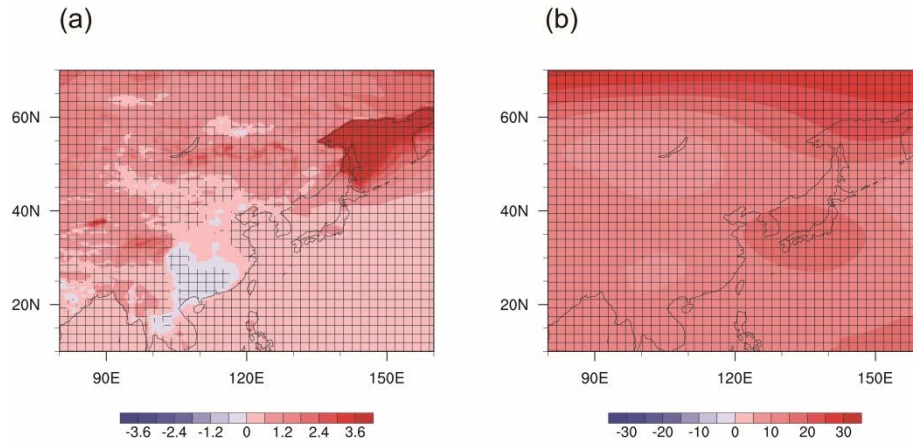
463 Figure 1 Climatology of winter-mean (DJF) (a) surface air temperature (shading, °C)

464 (c) 500 hPa geopotential height (shading, m) during 1960–2012, based on NCEP

465 reanalysis data. (b), (d) As in (a), (c), but for the model's All-Hist runs. (e)
 466 Taylor diagram of winter-mean climatology for surface air temperature (TAS;
 467 25°–45°N, 105°–145°E) and 500 hPa geopotential height (H500; 25°–45°N,
 468 105°–145°E). The rectangle marks the areas used to calculate the climatology in
 469 Taylor diagram.

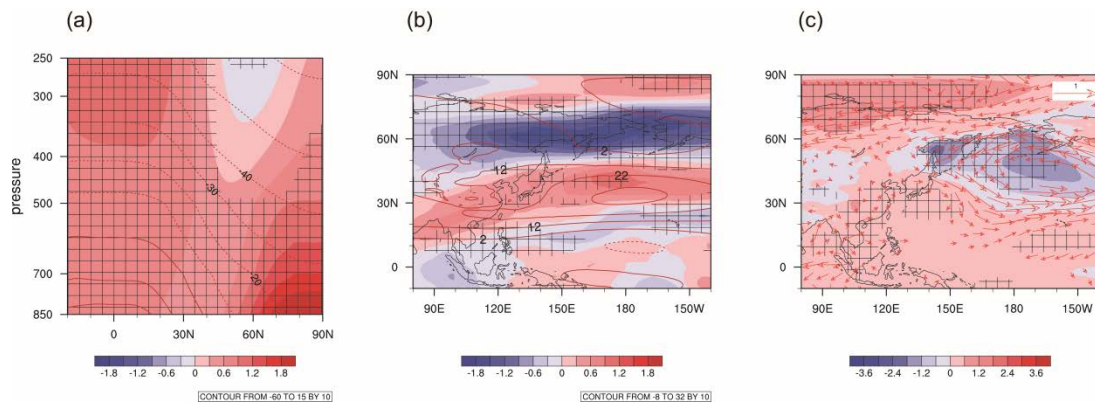


470
 471 Figure 2 (a) The time series of the normalized EAWMI_SAT (curve) and their linear
 472 trend (line) during 1960–2012, based on NCEP reanalysis dataset (top), outputs
 473 of model in All-Hist run (middle), and outputs of models in Nat-Hist run
 474 (bottom). (b) As in (a), but for the EAWMI_HGT. “tr” is an abbreviation for
 475 “linear trend coefficient”. “*” means the tr is significant at 95% confidence level
 476 based on the Mann-Kendall test, and “’ ” means the tr is significant at 90%
 477 confidence level. “cor” is an abbreviation for “correlation coefficient between
 478 simulated EAWM index under All-Hist scenario and observed EAWM index”,
 479 “cor_dec” is an abbreviation for “correlation coefficient in decadal time-scale”.
 480 Note that the time series of the EAWM indices base on outputs of model in the
 481 Nat-Hist runs are standardized by the climatology simulated by the All-Hist runs.



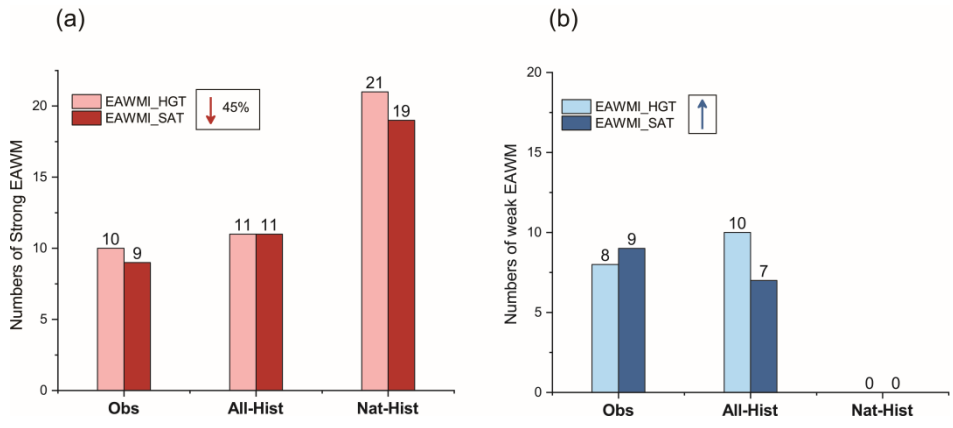
482

483 Figure 3 Composite differences of winter-mean (a) surface air temperature
 484 (shading, °C) and (b) 500 hPa geopotential height (shading, m) between the
 485 All-Hist runs and Nat-Hist runs, during 1960–2012. The plus signs denotes
 486 where the composite differences are significant at the 95% confidence level
 487 based on two-sided Student *t* test.



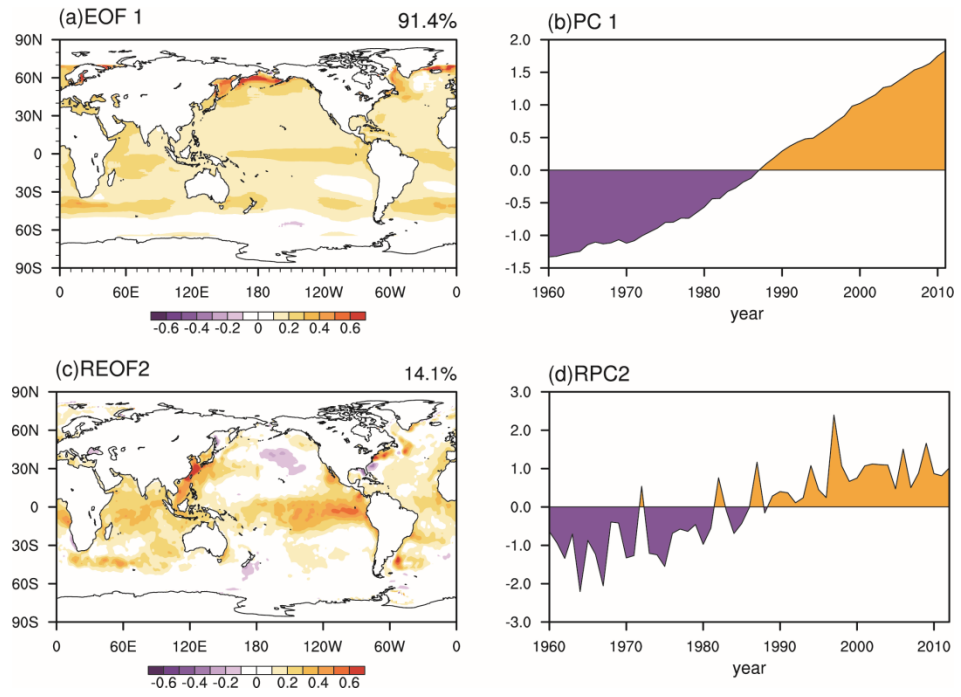
488

489 Figure 4 Composite differences of winter-mean (a) air temperature (shading, °C) over
 490 90°E–150°E, (b) 250 hPa zonal wind (shading, m/s) and (c) sea level pressure
 491 (shading, hPa) and 850 hPa wind (vector, m/s) between the All-Hist runs and
 492 Nat-Hist runs, during 1960–2012. Red contours denote the climatology of
 493 All-Hist runs. The plus signs denotes where the composite differences are
 494 significant at the 95% confidence level based on two-sided Student *t* test.



495
496
497
498
499

Figure 5 (a) The number of strong EAWM events during 1960–2012, based on NCEP reanalysis dataset (left), outputs of model in the All-Hist runs (middle), and outputs of model in the Nat-Hist runs (right). (b) As in (a), but for weak EAWM events.



500
501
502
503
504
505
506
507
508

Figure 6 The first leading mode (EOF1; a) and associated principal component (PC1; b) of the difference of the winter-mean sea surface temperature forcing between the All-Hist runs and Nat-Hist runs by empirical orthogonal function analysis based on the period of 1960-2013. The second leading mode (REOF2; c) and associated principal component (RCP2; d) of the winter-mean sea surface temperature from the HadISST data by rotated empirical orthogonal function analysis based on period of 1960-2013.